3D Printing of Transparent and Conductive Heterogeneous Hydrogel–Elastomer Systems

Kevin Tian, Jinhye Bae, Shannon E. Bakarich, Canhui Yang, Reece D. Gately, Geoffrey M. Spinks, Marc in het Panhuis, Zhigang Suo, and Joost J. Vlassak**

Interest in stretchable electronics has grown significantly in recent years, driving a need for soft and stretchable materials that can sustain high strains and still fulfill their function in applications such as human wearable sensors for biomechanics studies and health monitoring,[1–4] or feedback sensors in soft robotics.[5–8] Although many stretchable conductors exist, including liquid metals,[9,10] nanowires,[11,12] nanoribbons,[13] prestretched elastomer fibers with conductive coatings,[14] and microcracked metals,[15,16] these materials have generally been unable to achieve high levels of optical transparency while maintaining high conductivities and stretchability; a feature that would enable their use in optogenetics[17] or allow optical imaging of the underlying substrate. Conventional strategies of incorporating metallic components with elastomers to attain stretchability also yield nontrivial failure modes such as liquid metal leakage[8] and hard–soft material interfacial failure.[18] The use of gels as conductors, where ions are the charge carriers instead of electrons, represents an entirely different approach that has gained popularity recently. Their high stretchability and transparency, when combined with recent improvements in toughness and stiffness,[19,20] have already enabled their use as stretchable electrical conductors,[21,22] capacitive strain sensors,[23–25] and chemical/pH sensors.[26] Gel-based ionic circuits thus represent a unique class of devices within stretchable electronics. Conductive gels can be generally divided into those where the ions are provided by solvated salts[25,27] (hydrogels) or by ionic liquids[24,28,29] (ionogels). Although immune to dehydration, ionogels have comparatively lower conductivities than hydrogels. Ionic liquids also interfere with some gel polymerization reactions, limiting the range of polymers that can be used to synthesize ionogels.[30] By contrast, hydrogels are generally easier to synthesize, but they are susceptible to dehydration. Solvated hygroscopic salts may serve the dual purpose of increasing both their ionic conductivity and water-retention properties,[27] though a balance must be struck between maximizing water-retention and ionic conductivity due to nonidealities of the electrolyte solution that reduce molar conductivity at high salt concentrations.[31]

Fabrication of stretchable electronics using hydrogels requires integrating hydrogels with stretchable dielectrics such as dielectric elastomers; a process thus far primarily achieved via manual assembly of cast segments. If the field is to progress, advanced manufacturing techniques that integrate dielectric elastomers and hydrogels need to be developed.[7] Fabrication techniques specific to hydrogels have already been developed, including extrusion 3D printing,[24,32–35] digital projection based techniques,[36] and screen printing.[37,38] Extrusion printing techniques in particular are most easily capable of multi-material printing at high resolution and low costs.[33,34] Recently, Robinson et al. fabricated a soft sensor with an ionic-liquid based gel and a silicone elastomer by combining soft lithography with extrusion printing.[24] Although recent studies have successfully fabricated stretchable electronics consisting entirely of soft materials, conductive hydrogels and dielectric elastomers, thus far these fabrication techniques have relied on casting or a combination of extrusion printing with other methods.[21–25]

Here, we describe a simple approach to 3D extrusion printing of soft, stretchable electrical devices integrating a conductive hydrogel and a dielectric elastomer with sub-millimeter resolution. We show that both types of materials can be integrated into a single device using a single fabrication process. We characterize the mechanical and electrical performance of the printed hydrogel and demonstrate the technique by printing a soft strain sensor. The device was fabricated using poly(acrylamide) (PAAm) hydrogel and poly(dimethylsiloxane) (PDMS) because of their widespread use, as well as their

K. Tian, Dr. J. Bae, C. Yang, Prof. Z. Suo, Prof. J. J. Vlassak
School of Engineering and Applied Sciences
Harvard University
Cambridge, MA 02138, USA
E-mail: suo@seas.harvard.edu; vlassak@seas.harvard.edu

S. E. Bakarich, Prof. G. M. Spinks
School of Mechanical Materials and Mechatronic Engineering
University of Wollongong
Wollongong, NSW 2522, Australia

S. E. Bakarich, R. D. Gately, Prof. G. M. Spinks, Prof. M. in het Panhuis
Intelligent Polymer Research Institute
ARC Centre of Excellence for Electromaterials Science
AIIM Facility
University of Wollongong
Wollongong, NSW 2522, Australia

C. Yang
State Key Laboratory for Strength and Vibration of Mechanical Structures
International Center for Applied Mechanics
School of Aerospace
Xi'an Jiaotong University
Xi'an 710049, China

R. D. Gately, Prof. M. in het Panhuis
Soft Materials Group
School of Chemistry
University of Wollongong
Wollongong, NSW 2522, Australia

Prof. Z. Suo
Kavli Institute for Bionano Science and Technology
Harvard University
Cambridge, MA 02138, United States

DOI: 10.1002/adma.201604827

favorable electrical and optical properties. The hydrogel precursor consisted of a concentrated aqueous solution of a hygroscopic salt, a compatible rheological modifier, and UV-initiated polymerization/crosslinking compounds. Lithium chloride (LiCl) was selected as the hygroscopic salt in a compromise between vapor pressure and ionic conductivity, and its concentration (7 mol L^{-1}) was set above peak conductivity, but below saturation in an aqueous solution.[39] The PDMS was a UV curing formulation to allow for rapid setting during the printing process (KER-4690, courtesy of Shin-Etsu Silicones).

Printing was performed using an extrusion 3D printer comprised of a precision positioning system, an ink extrusion system, and a hardware/software interface to control location and rate of material extrusion relative to the sample stage (**Figure 1**a).[33] The entire system was housed inside a nitrogen environment. The relative humidity (RH) of the environment was fixed at 43% by bubbling nitrogen through a saturated solution of potassium carbonate.[40] Significant variations in RH during the fabrication process can lead to elastic instabilities in the hydrogel surface as a result of hydrogel swelling,[41] which can happen very quickly because of the high surface area to volume ratio of sub-millimeter features. Oxygen displacement was needed to prevent inhibition of the free-radical polymerization in the hydrogel precursor. In situ UV curing was used to partially set the extruded ink and prevent extensive spreading. This process is further elaborated during the discussion of rheological characteristics of the hydrogel precursor. Figure 1b demonstrates our printing capabilities of complex hydrogel–elastomer designs by comparing the final printing shape to its printing trace and Figure 1c highlights the optical transparency of the printed devices.

Selecting materials for extrusion printing requires the consideration of their rheological properties, since these properties dictate extrusion pressure, post-extrusion shape retention, and printing resolution. A shear-thinning characteristic is particularly desirable for extrusion, allowing for lowered viscosity under the high shear rates involved in extrusion and a higher viscosity post-extrusion for shape retention. Shear thinning is usually achieved through the addition of a rheological modifier, of which many are commercially available.[42] For this particular application, where the elastomer serves as a bulk dielectric as opposed to finer features, the resolution requirements for the extrusion printing of the PDMS are not as stringent as for the hydrogel. Consequently, the UV-curing PDMS formulation could be used without modification, despite its almost Newtonian behavior with viscosities of 4.8 Pa s at 0.1 s^{-1} and 4.5 Pa s at 10^2 s^{-1}. For applications where a higher resolution is required, many techniques and products are available to adjust the rheological behavior of the PDMS precursor.[5,24,43–47]

The development of the hydrogel precursor for our extrusion printing was more demanding and required a balance between conductivity, stability, and rheological characteristics. A significant proportion of rheological modifiers used in extrusion printing are sensitive to the ionic strength of the precursor,[33,34,48,49] and may lead to precipitation[50–52] or flocculation[53] of the rheological modifiers at the high salt concentrations necessary for good electrical conductivity and water retention. This requirement excludes many of the modifiers that are routinely used for hydrogel printing. High-molecular-weight polymers, however, are insensitive to the ionic strength of the precursor and have been used successfully in hydrogel extrusion printing.[24,35] In this study, we use high-molecular-weight PAAm as a rheological modifier, because of its transparency and compatibility with the precursor formulation.

The rheology of the PAAm/LiCl solution used to modify the flow characteristics of the precursor was characterized by measuring its viscosity (η), yield stress (σ_y), and viscoelastic moduli (G', G''). The precursor rheology is dominated

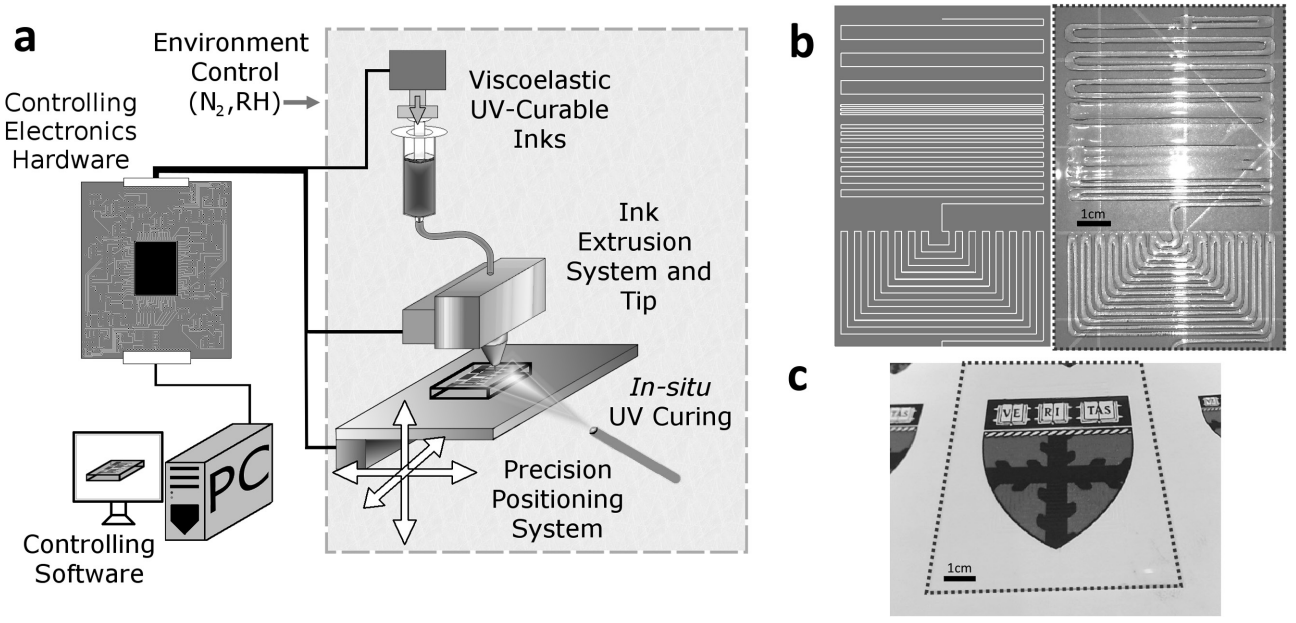

Figure 1. a) Overall schematic of the 3D printing extrusion system used in this study. b) A side-by-side comparison of a patterned design and the final printed hydrogel-on-PDMS sample. c) The same printed sample placed over an image to demonstrate its complete optical transparency.

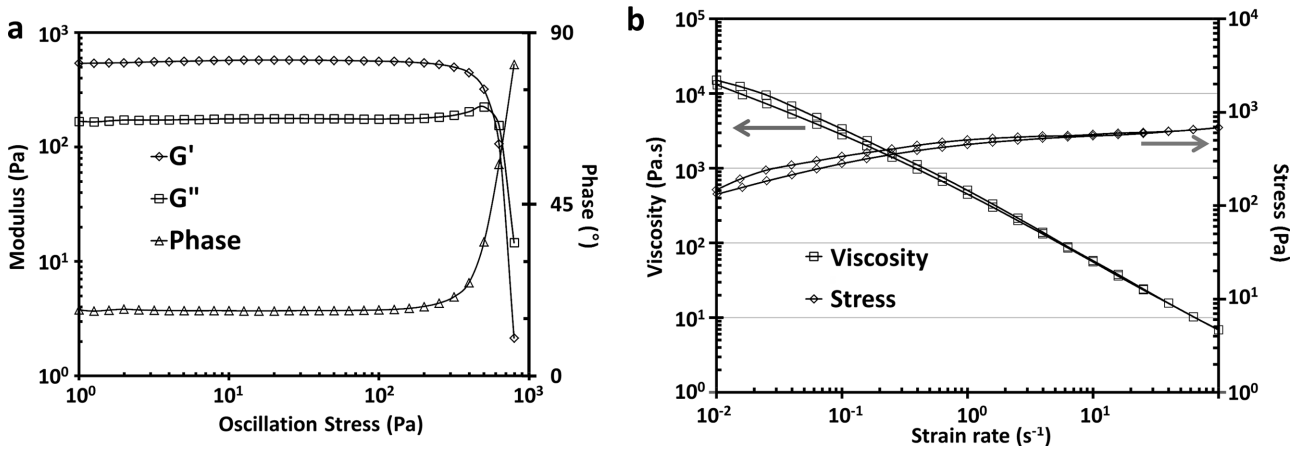

Figure 2. Rheological analyses of the rheological modifier for the hydrogel precursor. a) Typical oscillatory rheology results showing shear storage (G') and shear loss (G'') moduli evolution of inks used over increasing shear stress. b) Typical viscometry results showing stress and viscosity against shear rate. Tests were begun at low shear rates and swept up, then back down to demonstrate a mild thixotropic effect.

by the PAAm; all other components in solution do not affect the viscosity significantly at their respective concentrations. We performed both viscometry and oscillatory rheology (**Figure 2**) at 25 °C. The storage modulus (G') plateaus at a modulus of 558.5 ± 4.6 Pa and exceeds the loss modulus (G'') at shear stresses below 570 Pa, indicating solid-like behavior up to this stress level (Figure 2a); at stresses greater than 570 Pa, G'' exceeds G' and the precursor behaves more like a viscous liquid. Thus, the precursor has an apparent oscillatory yield stress of 570 Pa. Figure 2b depicts the stress and viscosity as a function of shear rate obtained from viscometry measurements. The viscosity shows clear shear-thinning behavior with $\eta \approx 15\,000$ Pa s at low shear rates (10^{-2} s^{-1}) and $\eta \approx 5$ Pa s at high shear rate (10^{2} s^{-1}). Extrapolating the linear portion of the stress-shear rate curve back to zero shear rates provides a Bingham yield stress of 458 Pa, which agrees well with the cross-over between G' and G''.

We estimate the shear-rate during extrusion using the generalized form of the Rabinowitsch–Mooney equation (Equation (1)) for a power-law fluid flowing through a cylindrical tube of radius r:[54]

$$\dot{\gamma} = \left(\frac{3n+1}{4n}\right)\frac{4Q}{\pi r^3} \tag{1}$$

where Q is the volumetric flow rate and n is the exponent of the power-law describing the shear stress as a function of shear-rate, $\tau = K\dot{\gamma}^n$, where K is the consistency index. By performing a power-law fit of the data in Figure 2b, we obtain a value of 0.148 for the shear-thinning exponent n in the high-strain rate region ($\dot{\gamma} > 1\,\text{s}^{-1}$). For a volumetric extrusion rate of 1 mm^3 s^{-1} and a 0.337 mm syringe tip diameter, the shear rate $\dot{\gamma}$ of the hydrogel precursor is ≈ 81 s^{-1}, with a corresponding viscosity of ≈ 7 Pa s. Immediately after extrusion, the viscosity increases to ≈ 1300 Pa s, assuming a shear rate of 0.1 s^{-1}. Other studies have achieved extrusion printing with viscosities of 10 Pa s at 10^2 s^{-1} and 10^2–10^3 Pa s at 0.1 s^{-1} strain rates.[24,33,35,49] Typical values for oscillatory rheological parameters in hydrogel extrusion printed inks place $G' \approx 350$–3000 Pa and $\sigma_y \approx 500$–3000 Pa.[24,35]

Our precursor hydrogel compares favorably with these other systems in terms of rheological performance. However, the precursor viscosity/G' values are insufficient to ensure printed shape retention over long periods of time. Since the hydrogel is UV curable, the simplest solution is to implement in situ UV curing during the extrusion printing process to partially cure the inks as they are extruded from the syringe tip (Figure 1a). Various hydrogel line geometries were generated by printing line stacks in both the lateral and vertical directions (**Figure 3**a), specified as the x and z-directions respectively, at constant extrusion rate, stage velocity, and lateral/vertical center-to-center spacing (6.0 mm^3 s^{-1}, 7.5 mm s^{-1}, S_x = 0.3 mm and S_z = 0.15 mm respectively). To precisely design 3D structures of hydrogel printed directly on PDMS, we characterized the geometry of the printed hydrogel structures in terms of the number of lines (N_x and N_z) in the x and z-directions, respectively (Figure 3b,c). We note that the degree of spreading in the x-direction increases with N_z, but that the spreading saturates once three layers have been printed, indicating that building up stable 3D structures is possible. The spreading of the hydrogel precursor post-extrusion is governed by a balance between capillary, viscous, and inertial forces acting on the extruded geometries. We may determine the dominant force using the Ohnesorge number,[55] $\text{Oh} = \eta/\left(\sqrt{\rho\gamma L}\right)$, where, γ is the surface energy, ρ is the mass density, and L the characteristic length scale. Using conservative values, $\eta \approx 10^3$ Pa s, $\gamma \approx 0.1$ J m^{-2}, $\rho \approx 10^4$ kg m^{-3}, and $L \approx 10^{-3}$ m, we observe that Oh ≈ $10^3 \gg 1$, indicating dominance of the viscous forces, as expected by the rheological design of the hydrogel precursor. The minimum level of lateral spreading was 0.8 mm, which can be observed by extrapolating Figure 3c to the y-intercept. This value can be decreased further by tuning the precursor rheology, increasing the in situ UV curing intensity, lowering the extrusion rates (Figure S1, Supporting Information), increasing the stage speed, or by utilizing a smaller size of syringe tip. Optical microscopy images of multilayer gel patterns showed smoothly merged surfaces (Figure 3d–f) and the formation of what are believed to be residual wetting layers on the hydrogel edges. Optical profilometry was used to obtain cross-sectional profiles

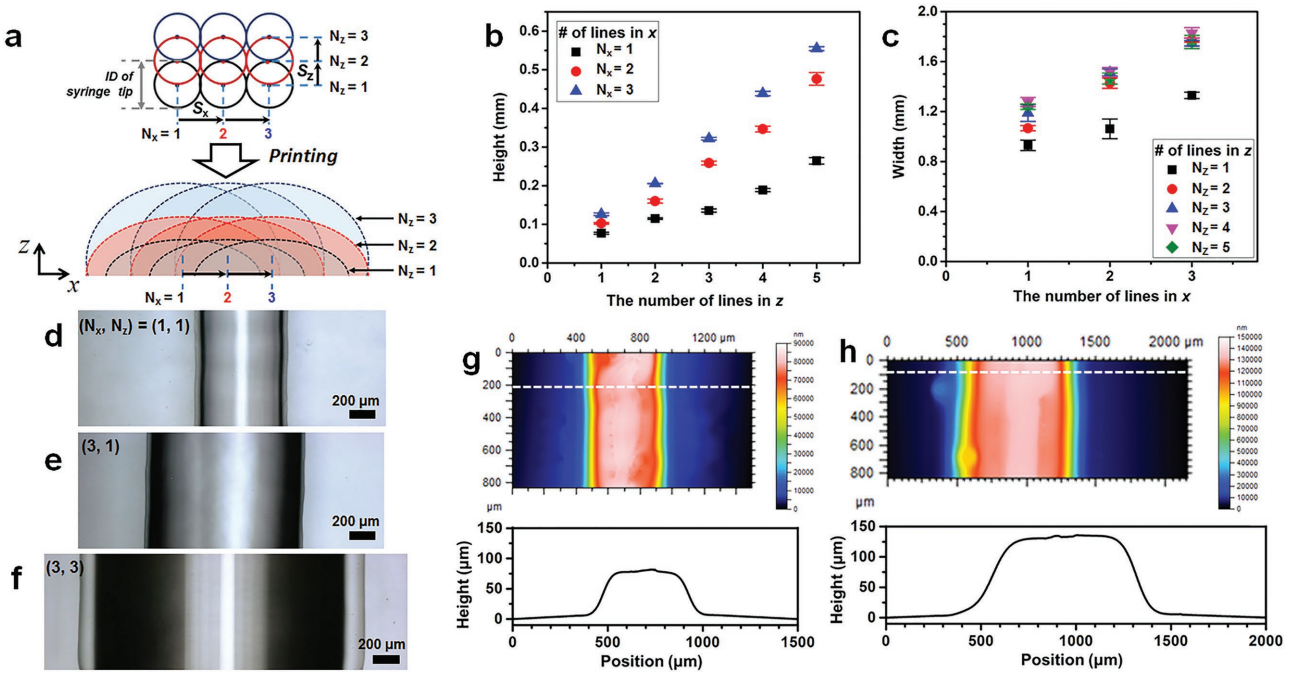

Figure 3. a) Schematic illustration of the extrusion trace and the resulting geometry of multiple lines separated both laterally, by S_x in the x direction, and vertically, by S_z in the z direction. The number of lines in x and z is (N_x,N_z) = (3, 3), respectively. b) Height of gel lines as a function of N_z. c) Width of gel lines as a function of N_x. Optical microscopy images of stacked layers of gel lines with d) (N_x, N_z) = (1, 1), e) (3, 1), and f) (3, 3). Optical profilometry images and the cross-sectional profiles of gel lines with multiple hydrogel layers of g) (1, 1) and h) (3, 1).

of the printed hydrogel lines (Figure 3g,h), which demonstrate that these profiles are nearly identical, indicating the reproducibility necessary for us to design and build 3D hydrogel structures.

Electrical testing of bulk cast hydrogel samples was conducted using a four-point probe configuration to establish the baseline electrical conductivity of the hydrogel. As shown in **Figure 4**a, we observed Ohmic conduction with a conductivity of 10.39 ± 0.31 S m^{-1}, which is comparable to the conductivity of the corresponding aqueous salt solution.[39] By contrast, the conductivity of the printed lines, measured under conditions of controlled humidity at RH 43%, was found to be 2.90 ± 0.40 S m^{-1}. This value is markedly lower than the bulk conductivity, but is most likely due to water loss post-extrusion. Although hydrogel water loss in open air will not be entirely avoided without the use of a sealant, such as by coating the hydrogel in an elastomer, the LiCl will allow the hydrogel to remain stable at a RH determined by the salt species and concentration. An aqueous LiCl solution increasing in mass percentage from 20 to 30% suffers a conductivity loss of 14%[39] and the volumetric change from water loss alone would cause a 62% decrease in cross-sectional area, which together approximates conductivity loss to be at least 48%. We characterized the resistance change of printed hydrogel lines printed on PDMS upon application of uniaxial tensile strain. The ideal case can be reasoned as follows: we let R and L, respectively be the resistance and length of a hydrogel line, and indicate their initial values with a subscript zero. We assume that the hydrogel is incompressible and the resistivity is independent of stretch. These assumptions predict that the ratio of resistance of the stretched hydrogel over the initial, unstretched resistance is given by $R/R_0 = (L/L_0)^2$. When the printed hydrogel lines are stretched by mechanically loading the PDMS, their resistance values obey this relationship up to rupture of the samples at 50% strain (Figure 4b). This result suggests that the hydrogel lines are intact up to this strain, since damage in the hydrogel would cause a deviation from this expression. Tensile tests on freestanding hydrogel samples show that the printed gel is capable of stretching up to 150% strain before rupture, further supporting the notion that the PDMS is the mechanically limiting component in this case. One could feasibly substitute PDMS with an alternative commercially available silicone elastomer for greater stretchability; silicone elastomers are generally compatible with the surface and rheological modification techniques used in this study. We also performed a fatigue test on a PDMS–hydrogel sample over the strain range from 0 to 20% for one thousand cycles, and measured the resistance of the hydrogel at logarithmic time intervals. Remarkably, there were no observable changes to the resistance of the device, nor were there visible signs of delamination (Figure 4c). We believe that the adhesion is primarily physical in nature; no chemical bonding between the two networks is possible given the lack of active sites. While PDMS surface oxidation treatments are known to degrade over time, this hydrophobic recovery is significantly inhibited by contact with water.[56–58] Given the high water content of hydrogels, their direct contact with PDMS should impart a similar protection of the surface treatment.

To demonstrate transmission of alternating current (AC) electrical signals, we fabricated a simple analog to the ionic cable:[22] two parallel ionically conductive hydrogel wires were extruded onto a printed PDMS substrate, with the two terminals

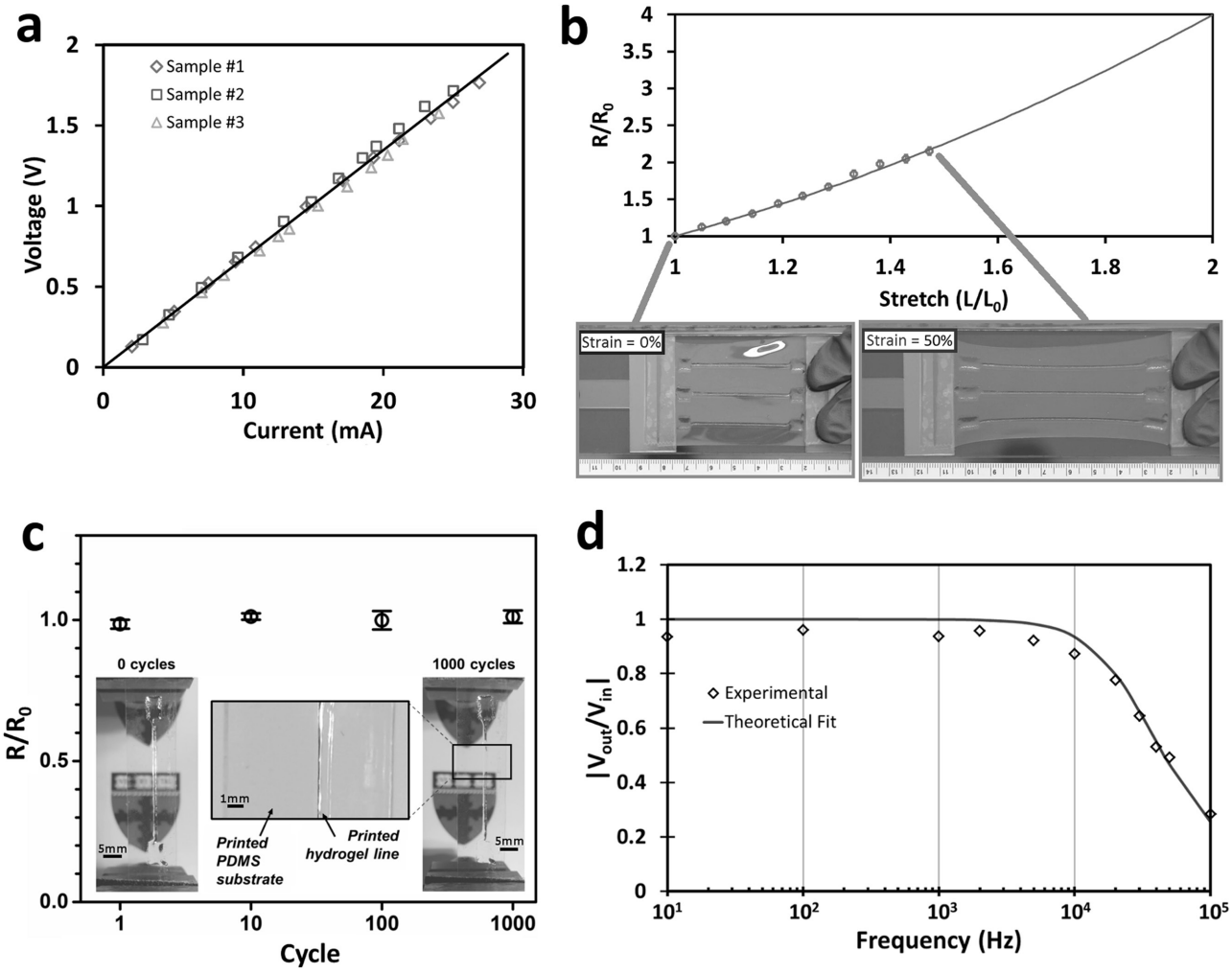

Figure 4. Electrical characterizations of the hydrogel in either bulk or printed state. a) *I–V* curves obtained from four-point probe measurements performed on bulk hydrogel samples. Sample dimensions were on average 30 cm long, 4.2 mm wide, and 3.5 mm in height, with an average measured resistance of 67.2 ± 2.4 Ω; this corresponds to a conductivity of 10.39 ± 0.31 S m^{-1}. b) The normalized resistance of printed hydrogels on a PDMS substrate is measured as a function of stretch, plotted against the ideal geometric behavior. Photos illustrate the sample in the initial (strain = 0%) state and stretched (strain = 50%) state with the mechanical load applied only to the PDMS. c) The normalized resistance of printed hydrogels on a PDMS substrate as a function of fatigue cycle number. Uniaxial tensile strain cycles of 20% strain were performed for up to 1000 cycles. No significant change to the resistance versus strain behavior was observed during our tests. Comparing images both before and after fatigue tests illustrate the lack of visible damage or delamination. d) The transfer function of an ionic cable design is plotted against frequency. We perform a theoretical fitting of our results using a simple RC circuit model for the ionic cable and can observe a reasonable level of agreement between experimental results and theory.

at either end serving as either an electrical input or output. The transfer function of the device was measured and fitted to a simple RC circuit model. Yang et al. demonstrated that the transmission of signals through an ionic conductor can be described using a special case of a transmission line model.[22] According to the theory of ionic cables, the condition for negligible decay of the signal is $(\omega\alpha\varepsilon l^2)/(bd) \ll 1$, where ω is the signal frequency, l is the cable length, b and α are the thickness and resistivity of the ionic conductor, and d and ε are the thickness and permittivity of the dielectric, respectively. Using representative values, $\varepsilon = 2 \times 10^{-11}$ F m^{-1}, $\alpha = 10^{-2}$ Ω m, $l = 10$ mm, $b = 50$ µm, $d = 50$ µm and let $\omega = 10^5$ s$^{-1} \approx 15$ kHz, we evaluate the expression to be 0.08, indicating negligible signal decay. Using a printed ionic cable with similar dimensions, we have successfully demonstrated signal transmission of AC signals up to 15 kHz in frequency (Figure 4d).

To demonstrate the capabilities of the printing process, we have extrusion printed a single-loop resistive strain gauge of hydrogel embedded within PDMS (**Figure 5**a). The sensor has a gauge factor of 0.84, and remains linear up to 40% strain (Figure S2, Supporting Information). The strain sensor was attached to the index finger of a nitrile glove using a thin layer of VHB brand adhesive tape (3M) and connected to a multimeter to measure the resistance of the sensor as it underwent varying degrees of strain as a result of the bending/flexing of the digits of the glove (Figure S3, Supporting Information). This sensing capability was extended to all five digits of a human hand (Figure 5). It can be observed that the strain gauge is sensitive

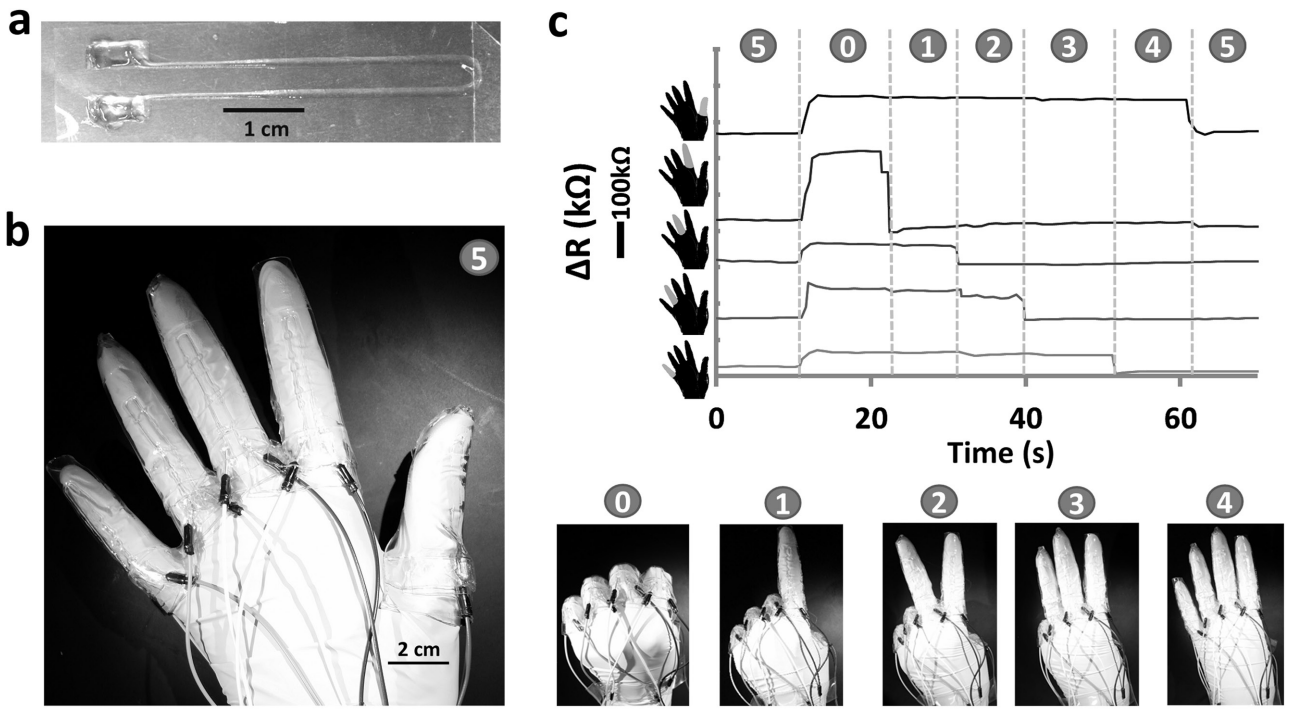

Figure 5. An example of a printed hydrogel–elastomeric type device, where fairly arbitrary shapes and designs can be easily integrated into the system by virtue of the printing process. In this case a) a simple resistance-based strain gauge is replicated using the hydrogel as the conductor and PDMS as the encapsulating substrate. b) By attaching the sensor to a flexible glove and flexing the digit we are able to observe a change in resistance up to 30% of its initial value at maximum finger bending and c) illustrate this process for a variety of hand gestures for each digit's strain sensor resistance change over time.

enough to detect inadvertent finger motions of the ring finger in position two (Figure 5c), as well as intermediate positions between being fully bent and fully straightened (Figure S3b, Supporting Information). We observed changes up to 30% in the strain gauge resistance at maximum finger bending, corresponding to an average strain of 36%. No delamination or fracture was observed during the experiment, verifying our previous results on the durability and stretchability of the printed laminates.

In conclusion, we have described a method for the 3D extrusion printing of an ionically conductive PAAm hydrogel and a PDMS dielectric elastomer to fabricate soft ionic devices. By tuning the rheological behavior of the hydrogel precursor and performing oxygen plasma treatments of PDMS surfaces, it is possible to print and integrate hydrogels directly with PDMS at sub-millimeter resolution. This capability was demonstrated by the fabrication and functional verification of an ionic cable and a resistance-based strain sensor. More complex geometries are readily designed and printed. The flexibility of the process allows one to replicate the design in an array or to print stacked devices for multi-axial strains. The strategies employed here to obtain the desirable printing resolution can be used for any hydrogel–PDMS material system. The PDMS may also be substituted with other commercially available silicone elastomers, since silicone elastomers are compatible with both the surface treatment and the rheological modification strategy used in this work. This study provides a simple pathway to the fabrication of hydrogels and dielectric elastomers in an integrated fashion for stretchable electrical devices and soft robotics applications.

Experimental Section

PDMS: A UV curable formulation of poly(dimethylsiloxane) elastomer (Shin-Etsu Silicones, KER-4690 A/B) was provided by the manufacturer as a two-part precursor and was used in the recommended 1:1 ratio. After a 2 min mixing cycle in a planetary centrifugal mixer (Thinky, ThinkyMixer ARE-300) at 2000 RPM, the precursor was used without further preparation and was cured via 365 nm UV light at a dose of 10 mW cm^{-2} for a period of 30 min, followed by an overnight bake at 65 °C. Prior to further printing, the PDMS was treated with an oxygen plasma (SPI Supplies, Plasma Prep II) at an O_2 pressure of 18 psi, vacuum pressure of 275 mTorr, and radio frequency (RF) power of 80 W for 60 s.

Preparation of the Hydrogel Precursor: The precursor used in the printing process consisted of two components: the rheological modifier and the hydrogel component. The rheological modifier consisted of an un-crosslinked PAAm solution made by UV exposing an acrylamide (AAm) (Sigma-Aldrich, A8887) solution containing α-ketoglutaric acid (α-keto) (Sigma–Aldrich,) and *N,N,N′,N′*-tetramethylethylenediamine (TEMED) (Sigma–Aldrich, T7024) at 25 °C with the following ratios (w/w): 92.17% deionized (DI) water (resistivity = 18.2 MΩ cm), 7.37% AAm, 0.00044% α-keto, 0.00021% TEMED. The hydrogel component consisted of AAm, α-keto, TEMED, lithium chloride (LiCl) (Sigma–Aldrich, 746460), and *N,N′*-methylenebis(acrylamide) (MBAA, Sigma–Aldrich, 146072). This component was added to the un-crosslinked PAAm solution and mixed using a planetary centrifugal mixer (Thinky, ThinkyMixer ARE-300) at 2000 RPM. Final precursor composition ratios (w/w) were: 63.15% deionized water, 3.86% PAAm, 9.05% AAm, 18.43% LiCl, 0.072% MBAA, 4.95% α-Keto, 0.479% TEMED.

Rheological Characterization: All rheological measurements were made using TA Instruments Discovery HR-3 Hybrid Rheometer with a cone and plate geometry at a reference temperature of 25 °C. Oscillatory

rheometry was performed on the PAAm/LiCl portion of the hydrogel precursor using a frequency of 1 Hz and sweeping shear stresses from 1 to 500 Pa. Viscometry was also performed with shear rates ranging from 0.01 to 100 s^{-1}.

Device Fabrication: PDMS and hydrogel precursors were directly printed onto a UV-resistant acrylic substrate (6.35 mm thickness, McMaster-Carr) rinsed with DI water followed by isopropyl alcohol and blown dry with nitrogen. A computerized numerical control (CNC) milling machine (Sherline Products, 5400) was used as a positioning stage, upon which independent linear actuators (Zaber Technologies, T-LA60A) were mounted onto the *z*-axis of the stage as syringe pumps. Syringes (5 mL, Hapool Medical Technology Co.) contained the precursors and were extruded through a 23 gauge blunted syringe tip (0.337 mm ID, SAI Infusion Technologies). A displacement rate was prescribed to the actuators and the requisite extrusion force was applied to the syringe end. A steady flow of dry nitrogen piped through a saturated potassium carbonate (Sigma–Aldrich) solution was used to purge the printing area of oxygen during the printing process and simultaneously fix the relative humidity. A 6 W UV LED (Instun, SK66) was used to initiate curing of the ink as it is extruded from the syringe at a dose rate of ≈3 mW cm^{-2}. Printed samples were then flood exposed to UV using an 8 W 365 nm UV Lamp (UVP, UVLS-28 EL) in a nitrogen environment at an effective dose rate of ≈6 mW cm^{-2}.

Devices began with a printed PDMS layer that was fully cured and baked, as previously described. Prior to additional printing, the PDMS was treated with O_2 plasma and stored in DI water until immediately prior to the printing in order to preserve the hydroxyl groups on the PDMS surface. While this plasma treatment process is incompatible with hydrogels already present on the PDMS due to vacuum requirements, a UV-Ozone treatment may be substituted to achieve the same effect at a slower rate while maintaining hydrogel integrity.[59] After subsequent hydrogel and PDMS layers were printed, the device was exposed to the flood UV lamp. Since the curing of PDMS has been observed to be inhibited by contact with the hydrogel precursor, the printed device was baked at 65 °C for 6 h to drive the PDMS curing process to completion, followed by a DI water soak of 1 h to rehydrate the hydrogel from the oven bake.

Sample Characterization: Cross-sectional images and measurements were made using a Coherence correlation interferometry (CCI) optical profiler (Taylor Hobson, CCI HD) with 5× and 20× objective lenses. Direct-current (DC) electrical measurements were made using multimeters (Fluke, models 8846A and 175). A DC power supply (Dr. Meter, PS-305DM) was used to generate the current used in the four-point probe measurement. For the AC characterization, a waveform generator (Keysight, 33500B) and oscilloscope (Keysight, DSO-1004A) with passive probes (Keysight, N2862B) were used. Uniaxial tensile testing, for both stress–strain and fatigue experiments, was performed on a uniaxial tensile tester (Instron, 3342 Single Column UTS) using a strain rate of 50 mm min^{-1}. For the fatigue experiments, a maximum strain of 20% was used. All PDMS–hydrogel samples were gripped using rubber-coated tensile grips in a region containing only PDMS. Stretch was calculated from the crosshead displacement rate and the initial gauge length of the samples.

Supporting Information

Supporting Information is available from the Wiley Online Library or from the author.

Acknowledgements

K.T. and J.B. contributed equally to this work. This research was supported by NSF (CMMI-1404653) and by the Harvard University MRSEC (DMR-1420570), University of Wollongong (SMAH Near-Miss Grant and SMAH/AIIM Travel Grants), and the Australian Research Council Centre of Excellence for Electromaterials Science (CE140100012). C.Y. was supported by the China Scholarship Council as a visiting scholar at Harvard University. This work was also performed in part at the Center for Nanoscale Systems (CNS), a member of the National Nanotechnology Coordinated Infrastructure Network (NNCI), which is supported by the National Science Foundation under NSF award no. 1541959. CNS is part of Harvard University.

Received: September 7, 2016
Revised: November 5, 2016
Published online:

[1] Y. S. Rim, S. H. Bae, H. Chen, N. De Marco, Y. Yang, *Adv. Mater.* **2016**, *28*, 4415.
[2] N. Lu, C. Lu, S. Yang, J. Rogers, *Adv. Funct. Mater.* **2012**, *22*, 4044.
[3] A. K. Bansal, S. Hou, O. Kulyk, E. M. Bowman, I. D. W. Samuel, *Adv. Mater.* **2015**, *27*, 7638.
[4] A. Lymberis, A. Dittmar, *IEEE Eng. Med. Biol. Mag.* **2007**, *26*, 29.
[5] J. T. Muth, D. M. Vogt, R. L. Truby, Y. Mengüç, D. B. Kolesky, R. J. Wood, J. A. Lewis, *Adv. Mater.* **2014**, *26*, 6307.
[6] A. Frutiger, J. T. Muth, D. M. Vogt, Y. Mengüç, A. Campo, A. D. Valentine, C. J. Walsh, J. A. Lewis, *Adv. Mater.* **2015**, *27*, 2440.
[7] M. Amjadi, K.-U. Kyung, I. Park, M. Sitti, *Adv. Funct. Mater.* **2016**, *26*, 1678.
[8] Y. Mengüç, Y.-L. Park, E. Martinez-Villalpando, P. Aubin, M. Zisook, L. Stirling, R. J. Wood, C. J. Walsh, *2013 IEEE Int. Conf. on Robotics and Automation (ICRA 2013)*, IEEE, Piscataway, NJ, USA, p. 5309; DOI: 10.1109/ICRA.2013.6631337.
[9] M. D. Dickey, R. C. Chiechi, R. J. Larsen, E. A. Weiss, D. A. Weitz, G. M. Whitesides, *Adv. Funct. Mater.* **2008**, *18*, 1097.
[10] A. Tabatabai, A. Fassler, C. Usiak, C. Majidi, *Langmuir* **2013**, *29*, 6194.
[11] S. Gong, W. Schwalb, Y. Wang, Y. Chen, Y. Tang, J. Si, B. Shirinzadeh, W. Cheng, *Nat. Commun.* **2014**, *5*, 3132.
[12] H. Yabu, K. Nagamine, J. Kamei, Y. Saito, T. Okabe, T. Shimazaki, M. Nishizawa, *RSC Adv.* **2015**, *5*, 88414.
[13] X. Feng, B. D. Yang, Y. Liu, Y. Wang, C. Dagdeviren, Z. Liu, A. Carlson, J. Li, Y. Huang, J. A. Rogers, *ACS Nano* **2011**, *5*, 3326.
[14] Z. F. Liu, S. Fang, F. A. Moura, J. N. Ding, N. Jiang, J. Di, M. Zhang, X. Lepró, D. S. Galvão, C. S. Haines, N. Y. Yuan, S. G. Yin, D. W. Lee, R. Wang, H. Y. Wang, W. Lv, C. Dong, R. C. Zhang, M. J. Chen, Q. Yin, Y. T. Chong, R. Zhang, X. Wang, M. D. Lima, R. Ovalle-Robles, D. Qian, H. Lu, R. H. Baughman, *Science* **2015**, *349*, 400.
[15] S. P. Lacour, S. Wagner, Z. Huang, Z. Suo, *Appl. Phys. Lett.* **2003**, *82*, 2404.
[16] Y. Xiang, T. Li, Z. Suo, J. J. Vlassak, *Appl. Phys. Lett.* **2005**, *87*, 161910.
[17] I. R. Minev, P. Musienko, A. Hirsch, Q. Barraud, N. Wenger, E. M. Moraud, J. Gandar, M. Capogrosso, T. Milekovic, L. Asboth, R. F. Torres, N. Vachicouras, Q. Liu, N. Pavlova, S. Duis, A. Larmagnac, J. Vörös, S. Micera, Z. Suo, G. Courtine, S. P. Lacour, *Science* **2015**, *347*, 159.
[18] Z. Suo, *MRS Bull.* **2012**, *37*, 218.
[19] J.-Y. Sun, X. Zhao, W. R. K. Illeperuma, O. Chaudhuri, K. H. Oh, D. J. Mooney, J. J. Vlassak, Z. Suo, *Nature* **2012**, *489*, 133.
[20] J. Li, W. R. K. Illeperuma, Z. Suo, J. J. Vlassak, *ACS Macro Lett.* **2014**, *3*, 520.
[21] C. Keplinger, J.-Y. Sun, C. C. Foo, P. Rothemund, G. M. Whitesides, Z. Suo, *Science* **2013**, *341*, 984.
[22] C. H. Yang, B. Chen, J. J. Lu, J. H. Yang, J. Zhou, Y. M. Chen, Z. Suo, *Extrem. Mech. Lett.* **2015**, *3*, 59.
[23] J.-Y. Sun, C. Keplinger, G. M. Whitesides, Z. Suo, *Adv. Mater.* **2014**, *26*, 7608.

[24] S. S. Robinson, K. W. O'Brien, H. Zhao, B. N. Peele, C. M. Larson, B. C. Mac Murray, I. M. van Meerbeek, S. N. Dunham, R. F. Shepherd, *Extreme Mech. Lett.* **2015**, *5*, 47.
[25] C. Larson, B. Peele, S. Li, S. Robinson, M. Totaro, L. Beccai, B. Mazzolai, R. Shepherd, *Science* **2016**, *351*, 1071.
[26] G. Gerlach, M. Guenther, G. Suchaneck, J. Sorber, K.-F. Arndt, A. Richter, *Macromol. Symp.* **2004**, *210*, 403.
[27] Y. Bai, B. Chen, F. Xiang, J. Zhou, H. Wang, Z. Suo, *Appl. Phys. Lett.* **2014**, *105*, 151903.
[28] B. Chen, J. J. Lu, C. H. Yang, J. H. Yang, J. Zhou, Y. M. Chen, Z. Suo, *ACS Appl. Mater. Interfaces* **2014**, *6*, 7840.
[29] M. Li, J. Li, H. Na, J. J. Vlassak, *Soft Matter* **2014**, *10*, 7993.
[30] P. Kubisa, *Prog. Polym. Sci.* **2009**, *34*, 1333.
[31] M. R. Wright, *An Introduction to Aqueous Electrolyte Solutions*, John Wiley & Sons, Ltd, Chichester, UK **2007**.
[32] D. M. Kirchmajer, R. Gorkin, M. in het Panhuis, *J. Mater. Chem. B* **2015**, *3*, 4105.
[33] S. E. Bakarich, M. in het Panhuis, S. Beirne, G. G. Wallace, G. M. Spinks, *J. Mater. Chem. B* **2013**, *1*, 4939.
[34] S. E. Bakarich, P. Balding, R. Gorkin, G. M. Spinks, M. in het Panhuis, *RSC Adv.* **2014**, *4*, 38088.
[35] R. A. Barry, R. F. Shepherd, J. N. Hanson, R. G. Nuzzo, P. Wiltzius, J. A. Lewis, *Adv. Mater.* **2009**, *21*, 2407.
[36] H. Lee, N. X. Fang, *J. Vis. Exp.* **2012**, *69*, e4457.
[37] D. A. Pardo, G. E. Jabbour, N. Peyghambarian, *Adv. Mater.* **2000**, *12*, 1249.
[38] S. E. Shaheen, R. Radspinner, N. Peyghambarian, G. E. Jabbour, *Appl. Phys. Lett.* **2001**, *79*, 2996.
[39] *CRC Handbook of Chemistry and Physics*, 92nd ed., (Eds: W. M. Haynes, D. R. Lide), CRC Press, Boca Raton, FL, USA **2011**, pp. 5–73.
[40] L. Greenspan, *J. Res. Natl. Bur. Stand., Sect. A* **1977**, *81A*, 89.
[41] D. Chen, J. Yoon, D. Chandra, A. J. Crosby, R. C. Hayward, *J. Polym. Sci., Part B: Polym. Phys.* **2014**, *52*, 1441.
[42] D. B. Braun, M. R. Rosen, *Rheology Modifiers Handbook: Practical Use and Application*, William Andrew Publishing, Norwich, NY, USA, **1999**, pp. 71–191.
[43] T. Femmer, A. J. C. Kuehne, M. Wessling, *Lab Chip* **2014**, *14*, 2610.
[44] J. O. Hardin, T. J. Ober, A. D. Valentine, J. A. Lewis, *Adv. Mater.* **2015**, *27*, 3279.
[45] D. B. Kolesky, R. L. Truby, A. S. Gladman, T. A. Busbee, K. A. Homan, J. A. Lewis, *Adv. Mater.* **2014**, *26*, 3124.
[46] S. Grilli, S. Coppola, V. Vespini, F. Merola, A. Finizio, P. Ferraro, *Proc. Natl. Acad. Sci., USA* **2011**, *108*, 15106.
[47] T. J. Hinton, A. R. Hudson, K. Pusch, A. Lee, A. W. Feinberg, *ACS Biomater. Sci. Eng.* **2016**, *2*, 1781.
[48] B. Duan, L. A. Hockaday, K. H. Kang, J. T. Butcher, *J. Biomed. Mater. Res., Part A* **2013**, *101 A*, 1255.
[49] S. Hong, D. Sycks, H. F. Chan, S. Lin, G. P. Lopez, F. Guilak, K. W. Leong, X. Zhao, *Adv. Mater.* **2015**, *27*, 4035.
[50] K. Y. von Hippel, P. H. Wong, *Biochemistry* **1962**, *1*, 664.
[51] A.-M. Hermansson, E. Eriksson, E. Jordansson, *Carbohydr. Polym.* **1991**, *16*, 297.
[52] I. Donati, S. Paoletti, *Alginates: Biology and Applications*, Springer-Verlag, Berlin, Germany **2009**, pp. 1–53.
[53] A. Mourchid, E. Lécolier, H. Van Damme, P. Levitz, *Langmuir* **1998**, *14*, 4718.
[54] Q.-H. Nguyen, N.-D. Nguye, in *Continnuum Mechanics—Progress in Fundamentals and Engineering Applications*, (Ed.: Y. Gan), InTech, Rijeka, Croatia, **2012**, DOI: 10.5772/26091.
[55] G. H. McKinley, M. Renardy, *Phys. Fluids* **2011**, *23*, 127101.
[56] S. H. Tan, N. T. Nguyen, Y. C. Chua, T. G. Kang, *Biomicrofluidics* **2010**, *4*, 1.
[57] I.-J. Chen, a. E. Lindner, *Langmuir* **2007**, *23*, 3118.
[58] X. Ren, M. Bachman, C. Sims, G. P. Li, N. Allbritton, *J. Chromatogr. B: Biomed. Sci. Appl.* **2001**, *762*, 117.
[59] Y. Berdichevsky, J. Khandurina, A. Guttman, Y.-H. Lo, *Sens. Actuators, B* **2004**, *97*, 402.